



# Preparation and characterization of thiosemicarbazide functionalized graphene oxide as nanoadsorbent sheets for removal of lead cations

A. F. Hassan<sup>1</sup> · R. Bulánek<sup>2</sup>

Received: 6 October 2016 / Revised: 21 June 2018 / Accepted: 15 September 2018 / Published online: 22 September 2018  
© Islamic Azad University (IAU) 2018

## Abstract

A facial and novel method for removal of  $\text{Pb}^{+2}$  based on the appealing interaction between thiosemicarbazide-modified graphene oxide nanosheets and  $\text{Pb}^{+2}$  is reported in this work. Textural and chemical characterization of graphite, graphene oxide, esterified graphene oxide and thiosemicarbazide-modified graphene oxide nanosheets was investigated using thermogravimetric analysis (TGA), nitrogen adsorption at  $-196\text{ }^\circ\text{C}$ , transmission electron microscopy (TEM), X-ray diffraction (XRD) and Fourier transform infrared spectroscopy (FTIR). Adsorption of  $\text{Pb}^{+2}$  was confirmed by Langmuir model with maximum adsorption capacity of 192.7 mg/g for thiosemicarbazide-modified graphene oxide nanosheets at  $27\text{ }^\circ\text{C}$  and initial pH value of 5.0. Kinetic studies showed that the adsorption of lead ions on the solid adsorbents follows pseudo-first order and Elovich kinetic models. Regeneration of graphene oxide, esterified graphene oxide and thiosemicarbazide-modified graphene oxide nanosheets was studied using different eluents ( $\text{H}_2\text{O}$ , 0.1 M HCl, 0.1 M EDTA) at different pH values. Both of disodium salt of ethylenediaminetetraacetic acid (EDTA) and HCl solutions (0.1 M) are efficient eluents to desorb lead cations from the solid adsorbent surface. Desorption efficiency of HCl solution decreases with increasing its pH value.

**Keywords** Adsorption · Characterization · Environmental · Kinetics · Nanomaterials

## Introduction

Environmental pollution with heavy metals is still one of the major problems due to their increased discharge. Heavy metal toxicity can result in damaged or reduced mental and central nervous function, lower energy levels, and damage to blood composition, kidneys, lungs, liver and other vital organs. Lead ions commonly exist in industrial and agricultural wastewater, storage battery, fuels, printing pigments, photographic materials and explosive materials and acidic

leachate from landfill sites in relatively high concentration. Lead exposure causes impaired blood regeneration, hypertension, severe stomach ache, brain and kidney damage and even can cause miscarriage in pregnant women. Although a very low concentration of  $\text{Pb}^{+2}$  is very toxic (Zhu et al. 2016; Pourjavadi et al. 2016), the permissible level for  $\text{Pb}^{+2}$  in drinking water is 0.05 mg/L according to the US Environmental Protection Agency. Removal of lead ions from aqueous media can be achieved with many techniques including chemical precipitation, ion-exchange, electro-flotation, membrane filtration, reverse osmosis and adsorption. Adsorption on a solid surface is still the most important and useful method for removal of pollutants due to their high removal percentage, simple handling process and the ease of solid adsorbent recovery. Surface modification of the solid adsorbent is essential to raise the adsorption capacity for lead ions. Graphene oxide is a heavily oxidized graphene with C/O atomic ratio of  $\sim 2$ , and the presence of reactive oxygen functional groups facilitates its chemical functionalization (Pumera 2013). In recent years, the oxygen-containing hydroxyl, carbonyl, carboxyl and epoxy functional groups have been successfully utilized as adsorption sites for toxic heavy metal cations. Removal of heavy

Editorial responsibility: Josef Trögl.

**Electronic supplementary material** The online version of this article (<https://doi.org/10.1007/s13762-018-2002-6>) contains supplementary material, which is available to authorized users.

✉ A. F. Hassan  
asmz68@yahoo.com

<sup>1</sup> Department of Chemistry, Faculty of Science, University of Damanhour, Damanhour, Egypt

<sup>2</sup> Department of Physical Chemistry, Faculty of Chemical Technology, University of Pardubice, Studentská 573, 53210 Pardubice, Czech Republic



metal cations from aqueous media was investigated by many recent researchers based on the presence of hydroxyl and carboxylic function groups on graphene oxide surface (Yang et al. 2015; Wu et al. 2013). Graphene oxide combined with new function groups especially containing nitrogen and/or additional carboxylic group through composite formation or surface modification can enhance the removal capacity for cations (Li et al. 2013; Yu et al. 2013). In the past decade, many researchers take attentions to graphene oxide and graphene surface modification through chemical covalent and non-chemical methods. Different procedures were used in functionalization, such as amidation, cycloaddition, substitution, diazonium coupling, silanization and doping. (Kosynkin et al. 2009). Hummer's oxidation method followed by organic reactions is the most frequently used methods (Liu et al. 2013). Graphene oxide modified with amine groups showed an efficient adsorption for extraction of many cations such as  $\text{Ni}^{+2}$ ,  $\text{Zn}^{+2}$ ,  $\text{Pb}^{+2}$ ,  $\text{Cu}^{+2}$  and  $\text{Cd}^{+2}$ . Thiol-functionalized graphene oxide was also reported for efficient removal of  $\text{Pb}^{+2}$  using cysteamine as surface modifying agent (Yari et al. 2015). Allyl acetoacetate-grafted graphene oxide was successfully prepared with high capacity for  $\text{Hg}^{+2}$  removals from aqueous medium (Aghdam et al. 2016).

The main goal of the present work is to prepare a novel thiosemicarbazide-modified graphene oxide nanosheets (TSGO) from esterified graphene oxide (EGO) for removal of lead ions from aqueous media. Thiosemicarbazide characterized by its thermal stability and containing different function groups enables the binding with graphene oxide (GO) surface groups and the ability of heteroatoms to remove metal cations from aqueous media. Textural and surface chemical characterizations are established to take a complete picture for the prepared nano-adsorbent sheets, different experimental adsorption conditions, involving time, pH of adsorbate solution and concentration of  $\text{Pb}^{+2}$  solution, are investigated, and GO and EGO are compared with TSGO as adsorbents. Finally, desorption of lead for reactivation of solid adsorbents and recovering of lead are performed using different effluents, namely water, hydrochloric acid and disodium salt of ethylenediaminetetraacetic acid. The research work was started in Chemistry Department, Faculty of Science, Damanshour University, Egypt, at the beginning of 2016 and completed in Pardubice University, Czech Republic.

## Materials and methods

### Materials

Graphite powder with particle size about 30 nm and thiosemicarbazide were purchased from Sigma-Aldrich Co., Ltd., and lead nitrate was purchased from Alfa Aesar Co.

Ltd. All of the other chemical reagents used in the experiments are of analytical grade and were purchased from El-Nasr for pharmaceutical and chemical industry Co., Egypt, and used without further purification.

### Preparation of solid adsorbents

Graphene oxide was prepared by Hummer's method. A total of 1.0 g graphite powders and 1.0 g sodium nitrate were mixed in an ice bath, then 100 mL concentrated  $\text{H}_2\text{SO}_4$  (98%) was added. Under vigorous stirring, 8.0 g  $\text{KMnO}_4$  was gradually added and the temperature of the mixture was kept below 20 °C. The mixture was stirred at 35 °C. After 3 h, 120 mL distilled water was slowly added to the formed brownish pasty mixture. A total of 10 mL of 30%  $\text{H}_2\text{O}_2$  was added to the mixture, where colour of the formed solution became a brilliant yellow. The mixture was washed with 10% hydrochloric acid and deionized water to remove the residual acid. Finally, the resulting sample (GO) was dried at 70 °C under vacuum conditions.

In a reaction flask, 1.5 g of GO was mixed with 30 mL of absolute ethanol and 1.0 mL of concentrated  $\text{H}_2\text{SO}_4$  added dropwise with constant stirring. The solution was refluxed for 4 h. After refluxing, solution was cooled to room temperature. The solid adsorbent was filtered and washed with distilled water and dried at 80 °C to obtain EGO.

Esterified graphene oxide (0.5 g) was treated by 50 mL ethanol and 0.5 g of thiosemicarbazide in Pyrex flask and stirred for 30 min (Ahmed 2008). The mixture was refluxed for 5 h, in the presence of water cooler and then filtered, washed with ethanol followed by distilled water and dried in an oven at 80 °C for 12 h (TSGO).

### Characterization of solid adsorbents

Thermogravimetric analysis for G, GO, EGO and TSGO was performed using thermoanalyser apparatus (Shimadzu D-50, Japan) at a nitrogen flow rate of 50 mL/min and a heating rate of 10 °C/min up to 800 °C. Specific surface area ( $S_{\text{BET}}$ ,  $\text{m}^2/\text{g}$ ), total pore volume ( $V_{\text{T}}$ , mL/g) and average pore radius ( $\bar{r}$ , nm) were determined via nitrogen adsorption at -196 °C using NOVA2000 gas sorption analyser (Quantachrome Corporation, USA). Prior to adsorption, the adsorbents were degassed at 200 °C for 6 h under a reduced pressure of  $10^{-4}$  Torr. Transmission electron microscopy (TEM) was conducted on a JEOL-JEM-2100 electron microscope operated at 200 kV (Tokyo, Japan). The crystalline characteristics of G, GO, EGO and TSGO were determined using powder X-ray diffractometer (Shimadzu XD-1, Japan). About 60 mg of sample was run as a thin film on a standard glass slide and a diffractogram in the  $2\theta$  ranges 5–70 with a scanning rate 2°/min. Fourier transform infrared spectra of GO, EGO and TSGO were measured using Mattson

5000 FTIR spectrometer in the range between 4000 and 400  $\text{cm}^{-1}$ , where KBr discs were prepared in as the previously described.

## Pb(II) adsorption experiments

To evaluate the effect of the initial  $\text{Pb}^{+2}$  concentration, the experiments were conducted at the initial  $\text{Pb}^{+2}$  concentrations from 25 to 300 mg/L at conditions of 0.6 g/L adsorbent dosage, pH 5.0 and contact time 45 min. The concentration of metal ion in solutions was determined by GBC Sens. AAS (Dandenong, Victoria 3175, Australia). The adsorption capacity was calculated by the following equation

$$q_e = \frac{(C_o - C_e)V}{W} \quad (1)$$

where  $C_o$  and  $C_e$  are the initial and equilibrium concentrations (mg/L) of adsorbate solution, respectively;  $W$  is the weight (g) of adsorbent used; and  $V$  is the volume of working solution (L). The effect of the initial pH on  $\text{Pb}^{+2}$  removals was investigated over range from 1.0 to 7.0 using 0.1 M HCl or 0.1 M NaOH solutions to adjust the required pH value. To investigate the kinetics of  $\text{Pb}^{+2}$  adsorption, 0.07 g of adsorbent was mixed with 100 mL  $\text{Pb}^{+2}$  solutions at the initial concentration of 400 mg/L, and the mixture (initial pH  $5.0 \pm 0.1$ ) was stirred for a predetermined time intervals. The adsorption capacity of the adsorbent at time  $t$ ,  $q_t$  (mg/g), was calculated as follows (Ciesielczyk et al. 2015)

$$q_t = \frac{(C_o - C_t)V}{W} \quad (2)$$

where  $C_t$  (mg/L) is the liquid-phase concentration of  $\text{Pb}^{+2}$  at time  $t$ .

## Desorption experiments

To measure desorption of  $\text{Pb}^{+2}$  from GO, EGO and TSGO, the Pb-preloaded adsorbent samples were prepared as mentioned in adsorption experiment. The Pb-preloaded adsorbent was then added to 25 mL of desorption solution ( $\text{H}_2\text{O}$ , 0.1 M HCl or 0.1 M EDTA) followed by agitation for 3 h. The desorbed amount of  $\text{Pb}^{+2}$  was determined by AAS as well as in the case of adsorption experiments. Desorption experiment was performed using HCl solutions at different pH values. The desorption efficiency was calculated by the following equation (Liu et al. 2012)

$$\text{Desorption efficiency} = V \frac{C_d}{q_w} \times 100\% \quad (3)$$

where  $C_d$  (mg/L) is the concentrations of  $\text{Pb}^{+2}$  aqueous solutions after desorption from the adsorbent.  $V$  (L) is the

volume of the aqueous solutions.  $q$  (mg/g) is the adsorption capacity of the adsorbent.  $W$  (g) is the mass of the adsorbents.

## Results and discussion

### Solid adsorbents characterization

The adsorption capacity of graphene oxides is determined by their physical properties but is also strongly influenced by the chemical structure of their surface. Content of water in the adsorbents and thermal stability of heteroatoms as surface function groups were investigated by thermogravimetric analysis as shown in Fig. 1. TGA of pure graphite clearly shows that it is thermally stable up to 800 °C in the presence of nitrogen gas with weight loss only 3 rel.% at 100 °C which is related to small amount of moisture adsorbed on the surface of  $G$ . For GO, the first weight loss up to 100 °C is mainly attributed to the evaporation of saturated water adsorbed on GO due to the presence of polar surface function groups which enhance water molecules adsorption, as was evidenced in the literature several times by mass spectrometry coupled with TGA (Wu et al. 2013; Ramezanzadeh et al. 2016; Yan et al. 2016). Other weight loss (about 20% of mass) is distinguishable at around 250 °C. This loss is usually attributed to the decomposition of oxygen-containing functional groups such as  $-\text{COOH}$ ,  $-\text{OH}$  and  $-\text{O}-$  (Beceril et al. 2008). At higher temperatures, GO suffers from thermal decomposition (Wu et al. 2013). Both of EGO and TSGO showed a higher thermal instability at temperatures above 150 °C compared with GO due to the presence of more bulky groups created by esterification in case of EGO and thiosemicarbazide groups in case of TSGO. TGA results showed that functionalized graphene oxide is not stable at temperatures above 150 °C and loses its weight by decomposition of surface functional groups.

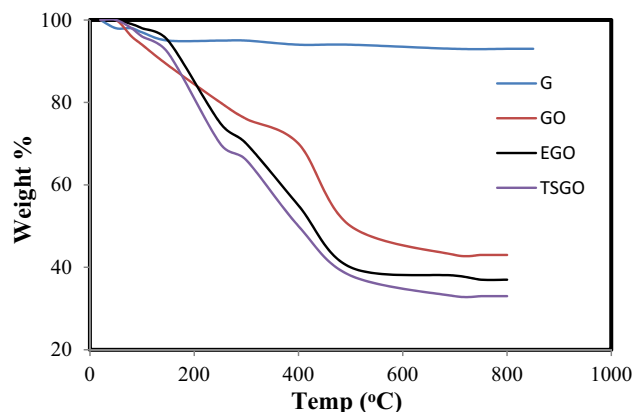


Fig. 1 TGA of G, GO, EGO and TSGO



The BET surface area ( $S_{\text{BET}}$ ,  $\text{m}^2/\text{g}$ ), total pore volume ( $V_{\text{T}}$ ,  $\text{mL}/\text{g}$ ) and pore radius ( $\bar{r}$ ,  $\text{nm}$ ) for GO, EGO and TSGO were estimated from BET analysis of the adsorption isotherms through nitrogen adsorption at  $-196\text{ }^\circ\text{C}$ . Upon analysis of data reported in Table 1, the main observation is that (i) surface area of functionalized GO materials (EGO and TSGO) is reduced by about 12% and 14% for EGO and TSGO, respectively, (ii) total pore volume of TSGO and EGO changed also as a result of pore blocking, but the relative decrease is lower than decrease in surface area (by 9% for TSGO and 5% for EGO in comparison with GO) and the same trend is also confirmed by the increase in the average pore radius. The previous results indicate that GO and its modified adsorbents are mesoporous materials (Fan et al. 2012).

Morphologies of GO, EGO and TSGO were examined using TEM. Figure 2 shows that GO sheets are very thin, quite smooth and homogeneous. After surface chemical modification (EGO and TSGO), the surface becomes wrinkled and folded, and this is related to the presence of more bulky surface groups which have a more hydrophobic nature (Lv et al. 2013).

Figure 3a shows XRD patterns of G, GO, EGO and TSGO. The sharp diffraction peak typical for graphite at  $2\theta=26.4^\circ$  ( $d=0.31\text{ nm}$ ) was observed in the XRD pattern of parent graphite material (Yang et al. 2015; Alok and Chauhan 2016). After oxidation, the characteristic graphite peak ( $2\theta=26.4^\circ$ ) disappears and is replaced by well-defined peaks at  $2\theta=10.9^\circ$  with  $0.81\text{ nm}$   $d$ -spacing. The increased

$d$ -spacing of GO sheets is due to swelling of the graphene sheets and the presence of abundant oxygen-containing functional groups on both sides of the graphene sheets causing an atomic-scale roughness on the graphene sheets (Li et al. 2013). EGO and TSGO show approximately the same characteristic peak of GO indicating that surface modification for GO with esters or thiosemicarbazide did not affect GO framework.

The surface modification of solid sorbents, such as graphene oxide with organic modifier, can be mainly interpreted based on FTIR analysis. Figure 3b shows the FTIR spectra for GO, EGO and TSGO between  $4000$  and  $400\text{ cm}^{-1}$ . GO has strong absorption band at  $3434\text{ cm}^{-1}$  corresponding to  $-\text{OH}$ . The peaks at  $1731$  and  $1633\text{ cm}^{-1}$  are corresponding to  $\text{C}-\text{O}$  stretching vibrations of  $-\text{COOH}$  groups and are contribution from aromatic  $\text{C}=\text{C}$  (Murugan et al. 2009), respectively. The bands located at  $1053$ ,  $1132$  and  $1440\text{ cm}^{-1}$  can be attributed to alkoxy, epoxy and carboxy groups, respectively (Wu et al. 2013). Esterification of carboxylic groups on GO with ethanol (EGO) was confirmed by the appearance of peak at  $1726\text{ cm}^{-1}$  which can be related to carbonyl of ester part and peak at  $2922\text{ cm}^{-1}$  indicating the presence of  $\text{C}-\text{H}$  stretching. TSGO curve shows the disappearance of the peak at  $1726\text{ cm}^{-1}$  which was related to carbonyl of ester group. The band appeared at  $1627\text{ cm}^{-1}$  is assigned to  $\text{C}=\text{S}$  amide stretching vibration and the band at  $1531\text{ cm}^{-1}$  is attributed to  $\text{C}=\text{N}$  stretching (Mohamed et al. 2013). The bands at  $3350$  and  $3300\text{ cm}^{-1}$  were attributed to  $-\text{NH}$  stretching,  $\nu(-\text{NH}_2)$  mode, respectively (Ahmed 2008; El-Metwally and Al-Hazmi 2013).

**Table 1** BET surface area, total pore volume and pore radius for GO, EGO and TSGO

Sample	$S_{\text{BET}}$ ( $\text{m}^2/\text{g}$ )	$V_{\text{T}}$ ( $\text{mL}/\text{g}$ )	$\bar{r}$ ( $\text{nm}$ )
GO	425	0.4120	1.8388
EGO	374	0.3881	2.0754
TSGO	365	0.3742	2.0504

## Adsorption of $\text{Pb}^{+2}$ from aqueous solution

### Effect of pH on the adsorption process

pH value plays an important role in the adsorption of  $\text{Pb}^{+2}$  on solid adsorbent. The effect of pH on the adsorption capacity was investigated over a wide range of pH (1.0–7.0) on

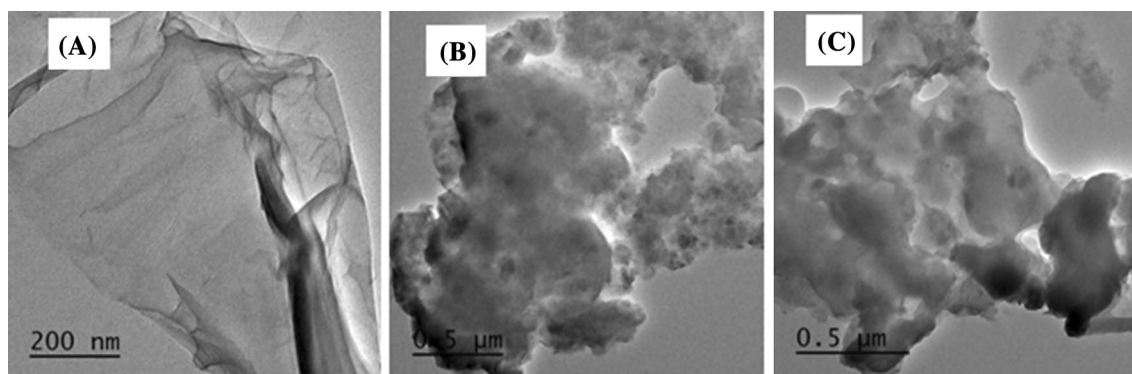


**Fig. 2** TEM images for GO (a), EGO (b) and TSGO (c)

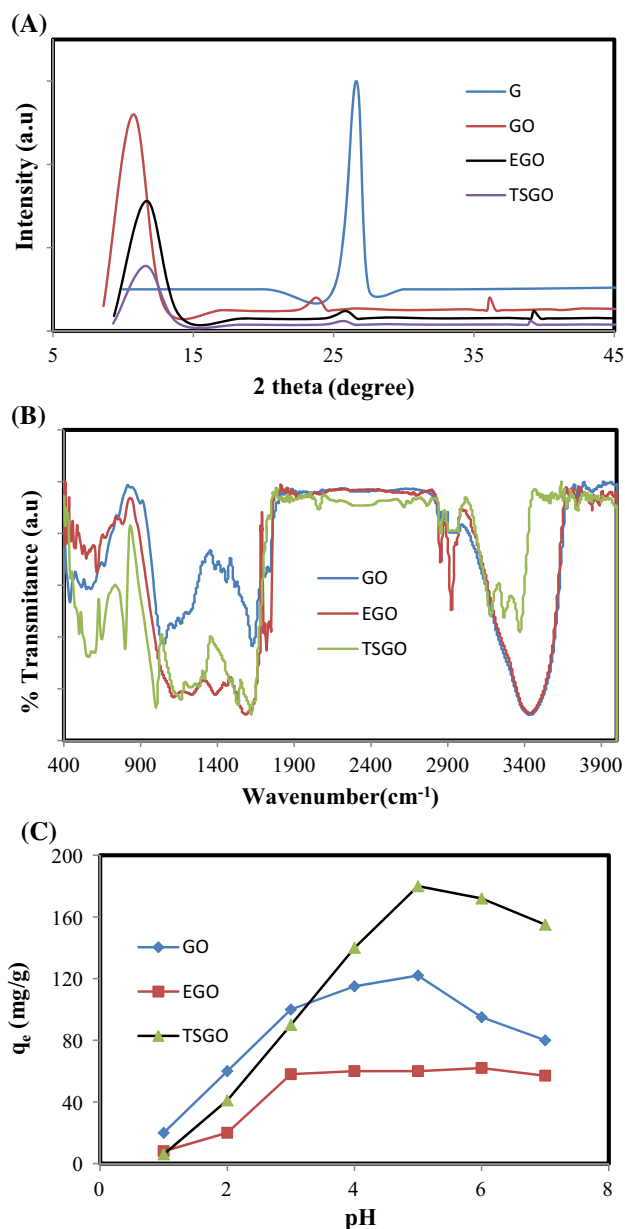


**Fig. 3** a XRD patterns of G, GO, EGO and TSGO, b FTIR spectra of GO, EGO and TSGO and c effect of pH on adsorption of  $Pb^{+2}$  onto GO, EGO and TSGO

avoid lead precipitation. In case of GO, lead adsorption steeply increases from 20.0 to 100.0 mg/g as the pH value increases from 1 to 3 and reaches the maximum value at pH 5.0 with 121.8 mg/g (Fig. 3c). This could be explained by the fact that  $-COOH$  and  $-OH$  groups of GO can be easily protonated at lower pH, inducing an electrostatic repulsion of  $Pb^{+2}$ . When pH values increase, the negative charge on the adsorbent increases and offers electrostatic attractions which are favourable for  $Pb^{+2}$ . That is also confirmed by observable decrease in the pH of adsorptive solution after the adsorption process. At pH higher than 5.0, there is a

slight decrease in  $Pb^{+2}$  uptakes until reaching 79.8 mg/g at pH 7.0. This slight decrease in  $Pb^{+2}$  uptake can be explained by hydrolysis of the lead cations at higher pH values resulting in repulsion with the negative sites on GO. The effect of pH on  $Pb^{+2}$  adsorption by EGO was not so strong due to the absence of  $-COOH$  groups and presence of only  $-OH$  group which are not so sensitive to the protonation. Increasing of lead uptake at pH values between 1.0 and 3.0 is not so distinct as for GO. Additional increase in pH value did not affect adsorption capacity. On the other hand, the introduction of nitrogen and sulphur atoms to TSGO surface enhances the effect of pH on the removal of lead cations. In case of TSGO as pH value increases from 1.0 to 5.0, a significant increase in the adsorption of  $Pb^{+2}$  was observed (it increases from 5.6 to 180.7 mg/g). This is because at lower pH the  $-NH_2$  and  $-NH$  groups on TSGO are easily protonated, inducing an electrostatic repulsion of  $Pb^{+2}$  (Fan et al. 2013).

#### Effect of contact time

Contact time is considered as an important parameter to investigate the kinetics of cation adsorption during wastewater treatment process. The effect of the contact time on the adsorption capacity of GO, EGO and TSGO for  $Pb^{+2}$  is shown in Fig. 4a. The adsorption equilibrium was attained after about 45, 34 and 30 min for GO, EGO and TSGO, respectively. The adsorption rate was high at the initial adsorption period of time, where adsorption capacity increased by about 9.0-fold and 3.7-fold from 5.0 to 30.0 min for TSGO and GO. These results might be due to the availability of large number of free sites that are saturated by time.

Adsorption kinetic studies were also conducted at different time intervals to study the rate of  $Pb^{+2}$  removals by adsorbents. It was applied to pseudo-first order (PFO), pseudo-second order (PSO) and Elovich adsorption kinetic models (Eqs. 4, 5 and 6, resp.).

$$\ln(q_e - q_t) = \ln(q_e) - (k_1 t) \quad (4)$$

$$\frac{t}{q_t} = \frac{1}{k_2 q_e^2} + \frac{1}{q_e} t \quad (5)$$

$$q_t = \frac{1}{\beta} \ln \alpha \beta + \frac{1}{\beta} \ln t \quad (6)$$

here  $q_e$  and  $q_t$  are the amounts of  $Pb^{+2}$  adsorbed (mg/g) at equilibrium and at time  $t$  (min), respectively,  $k_1$  is the PFO rate constant for adsorption ( $\text{min}^{-1}$ ) and  $k_2$  ( $\text{g/mg min}^{-1}$ ) is the rate constant of PSO adsorption.  $\alpha$  is the initial adsorption rate while  $\beta$  is related to activation energy for chemisorption and the extent of surface adsorption coverage.





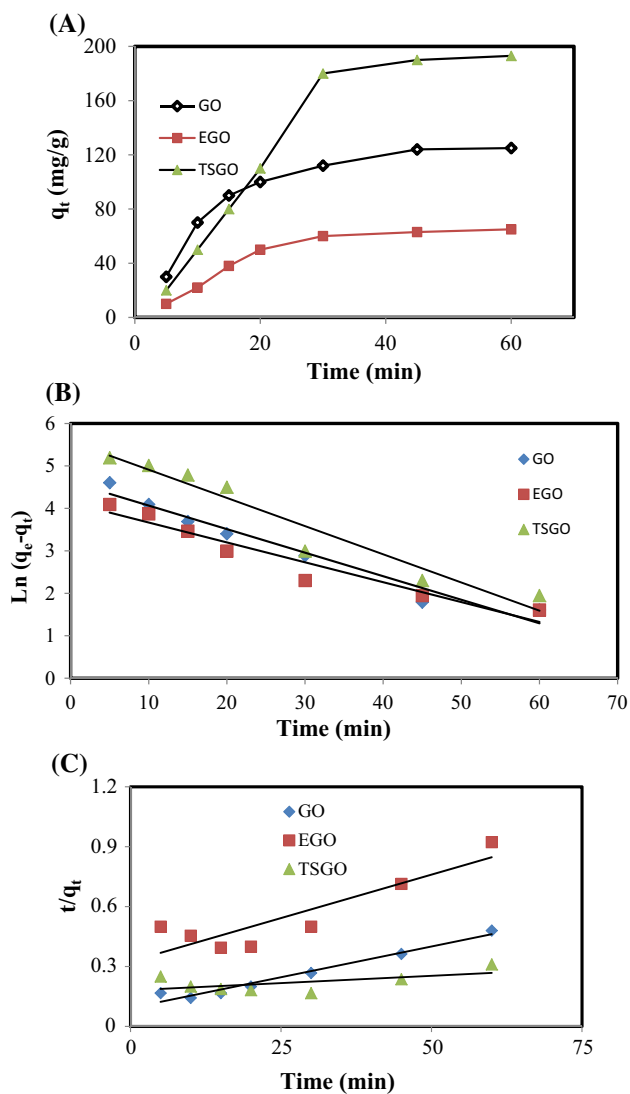


**Fig. 4** Effect of contact time (a), pseudo-first order (b), and pseudo-second order (c) plots for removal of  $Pb^{+2}$  by GO, EGO and TSGO

Figure 4b, c shows the linear plot of PFO and PSO kinetic models, respectively, while Suppl. 1 shows Elovich linear plot. Kinetic models parameters for adsorption of  $Pb^{+2}$  onto GO, EGO and TSGO are summarized in Table 2. The results from Table 2 show that (1) the adsorption of  $Pb^{+2}$  onto GO, EGO and TSGO follows PFO kinetic models based on the higher values of correlation coefficient calculated by PFO model and the small difference between the calculated and experimental values of adsorption capacity. (2) The PFO rate constants for adsorption ( $k_1$ ) values are 0.12725, 0.10794 and 0.15297 for GO, EGO and TSGO indicating that rate of adsorption for TSGO > GO > EGO which may be related to the abundance of surface function groups. (3) Correlation coefficients for all the solid adsorbents were found to be around 0.9520 indicating the good applicability of Elovich equation and confirm the chemisorption adsorption nature of  $Pb^{+2}$  by the solid adsorbents

**Table 2** Kinetic model parameters, Langmuir and Freundlich constants for adsorption of  $Pb^{+2}$  onto GO, EGO and TSGO at 27 °C

Sample		GO	EGO	TSGO
PFO	$q_e$ (mg/g)	110.6	67.2	236.1
	$K_1$ ( $min^{-1}$ )	0.12725	0.10794	0.15297
	$R^2$	0.9518	0.9165	0.9280
PSO	$q_e$ (mg/g)	162.3	114.8	684.5
	$K_2$ ( $g/mg \ min^{-1}$ )	0.18484	$4.9 \times 10^{-5}$	$7.7 \times 10^{-7}$
	$R^2$	0.1999	0.7576	0.9610
Elovich	$\alpha$ ( $mg \ g^{-1} \ min^{-1}$ )	22.009	7.518	17.550
	$\beta$ ( $mg/g$ )	0.02622	0.04138	0.01254
	$R^2$	0.95143	0.95191	0.95276
Langmuir	$q_m$ (mg/g)	124.4	67.9	192.7
	$R^2$	0.98636	0.95902	0.99735
	$b$ (L/mg)	0.20200	0.24520	0.21968
	$R_L$	0.0242	0.0199	0.0222
Freundlich	$K_F$ $mg/g \ (L/mg)^{1/n}$	38.49	23.07	49.80
	$n$	3.11	3.34	2.56
	$R^2$	0.88149	0.92013	0.92013

(Mohamed et al. 2016). (4) Initial adsorption rate for EGO is lower than that calculated for TSGO and GO which may be related to the abundance of adsorption active sites on TSGO and GO compared with EGO.

### Adsorption isotherms

The equilibrium adsorption isotherm describes the interactive behaviour between the adsorbate ions and the adsorbent active sites. Figure 5a shows the adsorption isotherms of lead ions onto GO, EGO and TSGO. It follows type I adsorption isotherms according to Sing classification. Type I isotherm is usually considered to be indicative of monolayer adsorption due to the strong adsorbent–adsorbate interactions, which involves chemical bonding between adsorbate and the adsorbent surface. The Langmuir and Freundlich models are the most abundant isothermal models (Li et al. 2013). The Langmuir isotherm, which assumes monolayer coverage on solid surface without subsequent interaction among adsorbed ions, is expressed as:

$$\frac{C_e}{q_e} = \frac{1}{bq_m} + \frac{C_e}{q_m} \quad (7)$$

$\frac{1}{bq_m}$ , where  $b$  (L/mg) is Langmuir constant,  $C_e$  (mg/L) is the equilibrium concentration,  $q_e$  (mg/g) is the amount adsorbed at equilibrium and  $q_m$  (mg/g) represents the monolayer capacity. A plot of  $\frac{C_e}{q_e}$  versus  $C_e$  gives a straight line (Fig. 5b) of slope  $\frac{1}{q_m}$  and intercept  $\frac{1}{bq_m}$ . The constants calculated from the linear form of Langmuir equation are given in Table 2. From data collected in Table 2, correlation coefficient values

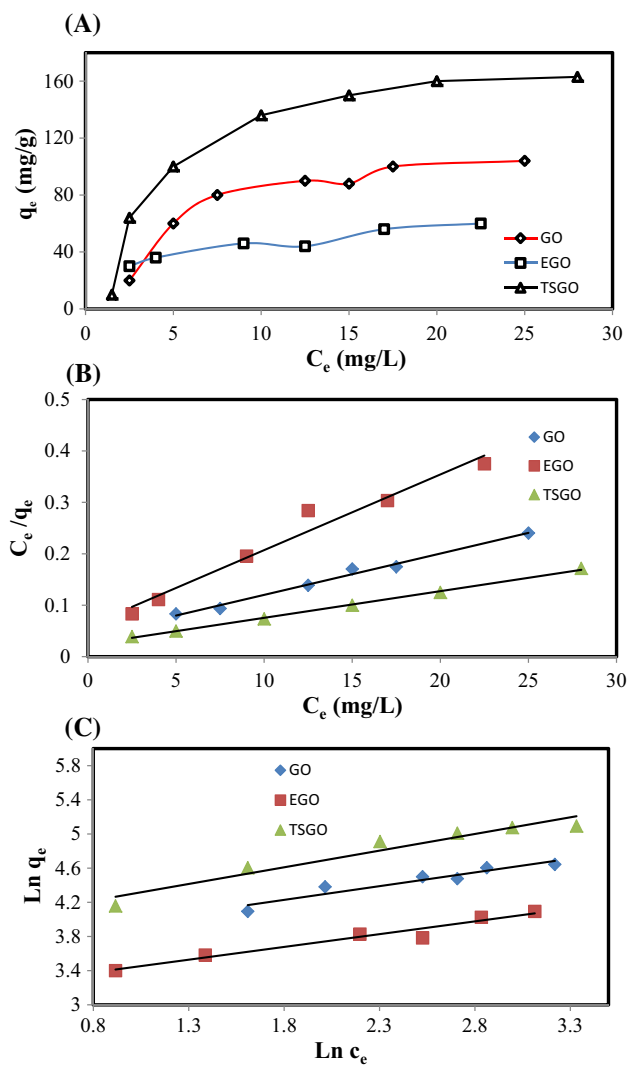


**Fig. 5** Adsorption isotherms (a), linear Langmuir plots (b) and Freundlich plots (c) for Pb<sup>2+</sup> adsorption on GO, EGO and TSGO at pH 5 and 27 °C

(> 0.95902) are indicating the good applicability of Langmuir adsorption model for Pb<sup>2+</sup> adsorption on GO, EGO and TSGO. Monolayer capacities for adsorbents follow the sequence TSGO > GO > EGO, which may be related to the abundances of surface function groups and agree well with adsorption capacities approximated from PFO kinetic model. Dimensionless separation factor  $R_L$  is defined as:

$$R_L = \frac{1}{1 + bC_0} \tag{8}$$

where  $b$  (L/mg) is the Langmuir constant and  $C_0$  (mg/L) is the initial Pb<sup>2+</sup> concentration. The value of  $R_L$  indicates the type of isotherm to be unfavourable ( $R_L > 1$ ), favourable ( $0 < R_L < 1$ ) or irreversible ( $R_L = 0$ ).  $R_L$  values for Pb<sup>2+</sup> adsorption onto GO, EGO and TSGO were less than unity and more than zero indicating favourable adsorption.

Figure 5c shows the Freundlich isotherm model for multi-layer adsorption on adsorbent. It can be expressed as:

$$\ln q_e = \ln K_F + \left(\frac{1}{n}\right) \ln C_e \tag{9}$$

$K_F$  (mg/g (L/mg)<sup>1/n</sup>) and  $n$  are the Freundlich constants characteristics of the system, indicating the adsorption capacity and the adsorption intensity, respectively. It is known that when the value of  $1/n$  is lower than one, it indicates a normal Langmuir isotherm; otherwise, it is an indicative of cooperative adsorption. Values of  $1/n$  are 0.322, 0.299 and 0.391 for GO, EGO and TSG, respectively, which is a good indicative for a normal Langmuir isotherm. Correlation coefficient ( $R^2$ ) calculated from Freundlich equation is lower than calculated from Langmuir equation (average value 0.9027), and in addition to that, the calculated adsorption capacity calculated from Freundlich model is far from that calculated from PFO kinetic model. From the last results, one can conclude that adsorption of Pb<sup>2+</sup> by GO, EGO and TSG follows Langmuir adsorption model.

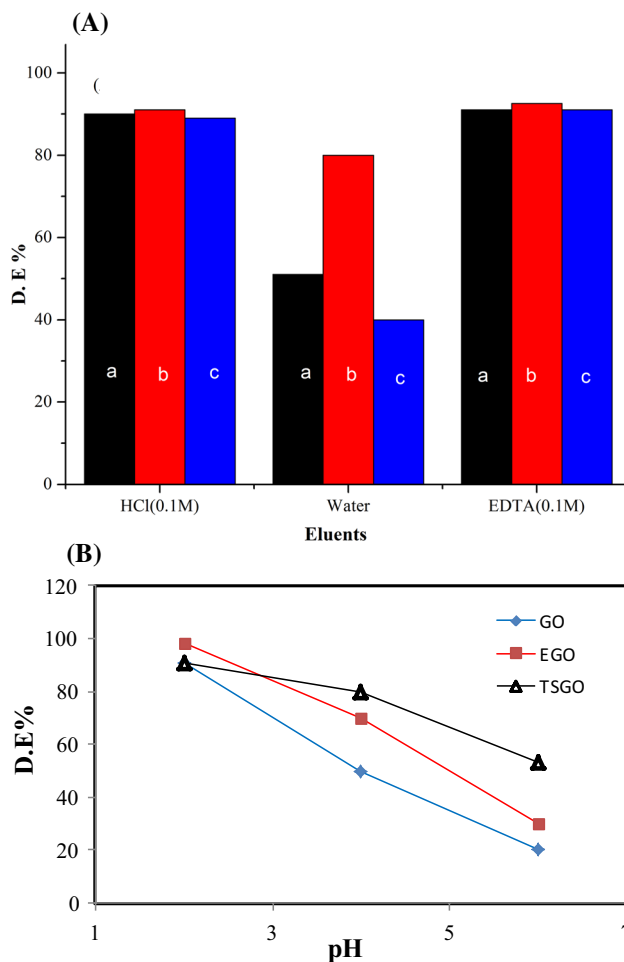


**Fig. 6** Desorption efficiency for adsorbed Pb<sup>2+</sup> using different eluents (A) and desorption efficiency at different pH values of HCl solutions (B) from preloaded GO (a), EGO (b) and TSGO (c)

## Desorption and reuse of solid adsorbents

It is important to regenerate and reuse solid adsorbents due to its high cost. Desorption experiments were performed using different solvents. Figure 6a shows desorption of  $Pb^{+2}$  from GO, EGO and TSGO using three different eluents ( $H_2O$ , 0.1 M aqueous solution of HCl and 0.1 M aqueous solution of EDTA). The desorption efficiency of  $Pb^{+2}$  eluted from the spent GO, EGO and TSGO is shown in Table 3. Upon inspection of data summarized in Table 3 can be concluded that (1) EDTA solution exhibits the highest efficacy of pre-adsorbed  $Pb^{+2}$  removal from surface of solid adsorbents, which may be related to the donation nature of EDTA molecule and the higher stability constant of lead EDTA complex. (2) HCl solution exhibits almost the same efficacy as the EDTA solution due to its polarity and the high tendency of  $Pb^{+2}$  to HCl. (3) Desorption efficiency of lead from adsorbents investigated follows the sequence TSGO < GO < EGO in all types of eluents used. Figure 6b shows dependence of desorption efficiency in HCl solutions at various pH values. It can be seen that desorption efficiency of HCl decreases with increasing pH value of HCl solution. Raising pH value to pH 6 reduces the desorption

efficiency into 20, 30 and 53% in case of TSGO, GO and EGO, respectively.

## Comparison with existing literature

Heavy metals removal, including lead cations, by adsorption has been studied on wide set of adsorbents such as modified graphene oxides, modified carbon nanotube, inorganic oxide, polyaniline-grafted-chitosan, charcoals,  $MgO-SiO_2$ , activated carbon and hydroxy sodalite (Moharram et al. 2016; Wang et al. 2016; Fan et al. 2013; Mukherjee et al. 2016; Wang et al. 2007; Ciesielczyk et al. 2016; Salvatore et al. 2016; Golbad et al. 2016). Activated carbons have undoubtedly been the most popular and widely used adsorbent in wastewater treatment. This study deals with functionalized graphitic materials. In order to have a broader perspective, adsorption capacities, desorption efficacy and some other characteristics of lead adsorption on various adsorbents are compared with adsorption characteristics of the materials reported in this study. For this purpose, Table 4 summarizes a relevant selection of data previously reported by several authors. Based on data reported in the literature, it is clear that adsorption capacity is usually far below 100 mg/g with the exception of tartaric acid-modified GO (Wang et al. 2016), sol/gel  $MgO-SiO_2$  (Ciesielczyk et al. 2016) and hydroxy sodalite (Golbad et al. 2016). Our adsorbent also exhibits very high desorption efficiency and mediocre equilibration time. We can conclude that our TSGO adsorbent reported here can be suitable and promising material for heavy metal removal, especially lead.

**Table 3** Desorption efficiency of  $Pb^{+2}$  from the surface of GO, EGO and TSGO using different eluents

Adsorbents	0.1 M HCl	$H_2O$	0.1 M EDTA
% Desorption efficiency			
GO	90.0	51.0	91.0
EGO	91.0	79.8	92.6
TSGO	89.0	39.8	91.0

**Table 4** Comparison of the maximum adsorption capacities, adsorption equilibrium time and desorption efficiency for lead onto TSGO with other adsorbents reported in previous researches

Adsorbents	Adsorption equilibrium time (min)	$q_m$ (mg/g)	Desorption efficiency (%)	References
Microspheres of graphene oxide (GO) crosslinked cellulose nanocomposites	250.0	22.22	59.9 (using 0.1 M EDTA)	Moharram et al. (2016)
Tartaric acid-modified graphene oxide	8.0	125.31	NA	Wang et al. (2016)
Water-dispersible magnetic chitosan/graphene oxide composites	60.0	76.94	90.1 (using 0.1 M HCl)	Fan et al. (2013)
Graphene oxide impregnated mixed matrix membrane	12.5	79.00	NA	Mukherjee et al. (2016)
Manganese oxide-coated carbon nanotubes	100.0	78.74	NA	Wang et al. (2007)
Sol-gel-derived inorganic oxide ( $MgO-SiO_2$ )	15.0	102.02	79.6 (using 0.05 M HCl)	Ciesielczyk et al. (2016)
Activated carbon	100.0	10.50	NA	Salvatore et al. (2016)
Hydroxy sodalite	120.0	153.84	NA	Golbad et al. (2016)
TSGO	30.0	192.70	91.0 (using 0.1 M EDTA)	(This study)

NA not applied



## Conclusion

In summary, GO was synthesized via Hummers method and functionalized with thiosemicarbazide after esterification with absolute ethanol. Characterization with TGA, nitrogen adsorption at  $-196\text{ }^{\circ}\text{C}$ , TEM, XRD and FTIR confirmed the differences between the three adsorbents and the successful modification of GO surface with thiosemicarbazide. Adsorption of lead ions with TSGO reaches its maximum value ( $192.7\text{ mg/g}$ ) at  $27\text{ }^{\circ}\text{C}$  and pH 5.0 after 30 min. Kinetic studies confirmed that the adsorption of lead ions onto the solid adsorbents follows pseudo-first order and Elovich kinetic models. High desorption capacity up to 92.6% in case of EGO is using 0.1 M EDTA solution. Nanoadsorbent sheets of TSGO are a promising solid adsorbent for adsorption of metal cations in a short time of application.

**Acknowledgements** This research was financed by the Research Sector of Damanhour University, Egypt and partially supported the Academy of Sciences of the Czech Republic (Institutional Project No. RVO: 68081723).

## References

- Aghdam K, Omayon H, Panahi A, Alaei E, Hasani AH, Moniri E (2016) Preparation of functionalized graphene oxide and its application as a nanoadsorbent for  $\text{Hg}^{2+}$  removal from aqueous solution. *Environ Monit Assess*. <https://doi.org/10.1007/s10661-016-5226-2>
- Ahmed SA (2008) Alumina physically loaded by thiosemicarbazide for selective preconcentration of mercury (II) ion from natural water samples. *J Hazard Mater* 156:521–529
- Alok PS, Chauhan Komal C (2016) Comparative studies on graphite and carbon black powders, and their dispersions. *J Mol Liq* 221:292–297
- Becerril HA, Mao J, Liu Z, Stoltenberg RM, Bao Z, Chen Y (2008) Evaluation of solution-recessed reduced graphene oxide films as transparent conductors. *ACS Nano* 2:463–470
- Ciesielczyk F, Bartczak P, Jesionowski T (2015) A comprehensive study of Cd(II) ions removal utilizing high surface-area binary Mg–Si hybrid oxide adsorbent. *Int J Environ Sci Technol* 12:3613–3626
- Ciesielczyk F, Bartczak P, Jesionowski T (2016) Removal of cadmium(II) and lead(II) ions from model aqueous solutions using sol–gel-derived inorganic oxide adsorbent. *Adsorption* 22(4):445–458
- El-Metwally NM, Al-Hazmi GAA (2013) Spectroscopic evaluation for VO(II), Ni(II), Pd(II) and Cu(II) complexes derived from thiosemicarbazide: a special emphasis on EPR study and DNA cleavage. *Spectrochim Acta Part A Mol Biomol Spectrosc* 107:289–295
- Fan L, Luo C, Sun M, Qiu H (2012) Synthesis of graphene oxide decorated with magnetic cyclodextrin for fast chromium removal. *J Mater Chem* 22(47):24577
- Fan L, Luo C, Sun M, Li X, Qiu H (2013) Highly selective adsorption of lead ions by water-dispersible magnetic chitosan/graphene oxide composites. *Colloids Surf B* 103:523–529
- Golbad S, Khoshnoud P, Abu-Zahra N (2016) Hydrothermal synthesis of hydroxy sodalite from fly ash for the removal of lead ions from water. *Int J Environ Sci Technol*. <https://doi.org/10.1007/s13762-016-1133-x>
- Kosynkin DV, Higginbotham AL, Sinitskii A, Lomeda JR, Dimiev A, Price BK, Tour JM (2009) Longitudinal unzipping of carbon nanotubes to form graphene nanoribbons. *Nature* 458:872–876
- Li L, Fan L, Sun M, Qiu H, Li X, Duan H, Luo C (2013) Adsorbent for chromium removal based on graphene oxide functionalized with magnetic cyclodextrin-chitosan. *Colloids Surf B* 107:76–83
- Liu L, Li C, Bao C, Jia Q, Xiao P, Liu X, Zhang Q (2012) Preparation and characterization of chitosan/graphene oxide composites for the adsorption of Au(III) and Pd(II). *Talanta* 93:350–357
- Liu Z, Zhou H, Huang Z, Wang W, Zeng F, Kuang Y (2013) Graphene covalently functionalized with poly(p-phenylenediamine) as high performance electrode material for supercapacitors. *J Mater Chem A* 1(10):3454–3462
- Lv M, Wang X, Li J, Yang X, Zhang C, Yang HuH (2013) Cyclodextrin-reduced graphene oxide hybrid nanosheets for the simultaneous determination of lead(II) and cadmium(II) using square wave anodic stripping voltammetry. *Electrochim Acta* 108:412–420
- Mohamed A, Ahamed R, Jeyakumar D, Burkanudeen AR (2013) Removal of cations using ion-binding terpolymer involving 2-amino-6-nitro-benzothiazole and thiosemicarbazide with formaldehyde by batch equilibrium technique. *J Hazard Mater* 248–249:59–68
- Mohamed EM, Gehan MN, Nabila ME, Heba IB, Sandeep K, Tarek MA (2016) Kinetics, isotherm, and thermodynamic studies of the adsorption of reactive red 195 A dye from water by modified Switchgrass Biochar adsorbent. *J Ind Eng Chem* 37:156–167
- Moharram MA, Tohami T, El Hotaby WM, Bakr AM (2016) Graphene oxide porous crosslinked cellulose nanocomposite microspheres for lead removal: kinetic study. *React Funct Polym* 101:9–19
- Mukherjee R, Bhunia P, De S (2016) Impact of graphene oxide on removal of heavy metals using mixed matrix membrane. *Chem Eng J* 292:284–297
- Murugan VA, Muraliganth T, Manthiram A (2009) Rapid, facial microwave-solvothermal synthesis of graphene nanosheets and their polyaniline nanocomposites for energy storage. *Chem Mater* 21:5004–5006
- Pourjavadi A, Abedin-Moghanaki A, Hosseini SH (2016) Synthesis of poly(amidoamine)-graft- poly(methyl acrylate) magnetic nanocomposite for removal of lead contaminant from aqueous media. *Int J Environ Sci Technol* 13:2437–2448
- Pumera M (2013) Electrochemistry of graphene, graphene oxide and other graphenoids. *Electrochem Commun* 36:14–18
- Ramezanzadeh B, Haeri Z, Ramezanzadeh M (2016) A facile route of making silica nanoparticles-covered graphene oxide nanohybrids ( $\text{SiO}_2\text{-GO}$ ); fabrication of  $\text{SiO}_2\text{-GO/epoxy}$  composite coating with superior barrier and corrosion protection performance. *Chem Eng J* 303:511–528
- Salvatore C, Antonio G, Demetrio M, Nicola M, Alberto P (2016) Pb(II) adsorption by a novel activated carbon–alginate composite material: kinetic and equilibrium study. *Int J Biol Macromol* 92:769–778
- Wang S, Gong W, Liu X, Yao Y, Gao B, Yue Q (2007) Removal of lead(II) from aqueous solution by adsorption onto manganese oxide-coated carbon nanotubes. *Sep Purif Technol* 58:17–23
- Wang Z, Yue B, Teng J, Jiao F, Jiang X, Yu J, Zhong M, Chen X (2016) Tartaric acid modified graphene oxide as a novel adsorbent for high-efficiently removal of Cu(II) and Pb(II) from aqueous solutions. *J Taiwan Inst Chem Eng* 66:181–190
- Wu W, Yang Y, Zhou H, Ye T, Huang Z, Liu R, Kuang Y (2013) Highly efficient removal of Cu(II) from aqueous solution by using graphene oxide. *Water Air Soil Pollut* 224:1372–1379
- Yan X, Qun G, Hongqin L, Kangsheng Z (2016) Effects of functional graphene oxide on the properties of phenyl silicone rubber composites. *Polym Test* 54:168–175



- Yang X, Li Y, Du Q, Sun J, Chen L, Hu S, Wang Z, Yanzhi X, Linhua X (2015) Highly effective removal of basic fuchsin from aqueous solutions by anionic polyacrylamide/graphene oxide aerogels. *J Colloid Interface Sci* 453:107–114
- Yari M, Rajab M, Moradi O, Yari A, Asif M, Agarwal S, Gupta VK (2015) Kinetics of the adsorption of Pb(II) ions from aqueous solutions by graphene oxide and thiol functionalized graphene oxide. *J Mol Liq* 209:50–57
- Yu B, Xu J, Liu J, Yang S, Luo J, Zhou Q, Wan J, Liao R, Wang H (2013) Adsorption behavior of copper ions on graphene oxide–chitosan aerogel. *J Environ Chem Eng* 1:1044–1050
- Zhu C, Dong X, Chen Z, Naidu R (2016) Adsorption of aqueous Pb(II), Cu(II), Zn(II) ions by amorphous tin(VI) hydrogen phosphate: an excellent inorganic adsorbent. *Int J Environ Sci Technol* 13:1257–1268

